JVST B
Journal of Vacuum Science & Technology B

Au-free recessed Ohmic contacts to AlGaN/GaN high electron mobility transistor: Study of etch chemistry and metal scheme

Cite as: J. Vac. Sci. Technol. B **38**, 032207 (2020); https://doi.org/10.1116/1.5144509
Submitted: 03 January 2020 . Accepted: 25 March 2020 . Published Online: 09 April 2020

Niranjan S, Ivor Guiney, Colin J. Humphreys, Prosenjit Sen, Rangarajan Muralidharan, and Digbijoy N. Nath

JVST B
Journal of Vacuum Science & Technology B

ARTICLE

avs.scitation.org/journal/jvb

Au-free recessed Ohmic contacts to AlGaN/GaN high electron mobility transistor: Study of etch chemistry and metal scheme

Cite as: J. Vac. Sci. Technol. B 38, 032207 (2020); doi: 10.1116/1.5144509
Submitted: 3 January 2020 · Accepted: 25 March 2020 ·
Published Online: 9 April 2020

Niranjan S,[1,a)] Ivor Guiney,[2] Colin J. Humphreys,[3] Prosenjit Sen,[1] Rangarajan Muralidharan,[1] and Digbijoy N. Nath[1]

AFFILIATIONS

[1]Centre for Nano Science and Engineering, Indian Institute of Science, Bangalore 560012, India
[2]Paragraf, West Newlands Industrial Park, Somersham PE28 3EB, United Kingdom
[3]School of Engineering and Materials Science, Queen Mary University of London, London E1 4NS, United Kingdom

[a)]**Electronic mail:** niranajans@iisc.ac.in

ABSTRACT

The authors study the effect of etch chemistry and metallization scheme on recessed Au-free Ohmic contacts to AlGaN/GaN heterostructures on silicon. The effect of variation in the recess etch chemistry on the uniformity of Ohmic contact resistance has been studied using two different etch chemistries (BCl_3/O_2 and BCl_3/Cl_2). Experiments to determine the optimum recess etch depth for obtaining a low value of contact resistance have been carried out, and it is shown that near-complete etching of the AlGaN barrier layer before metallization leads to the lowest value of contact resistance. Furthermore, two metal schemes, namely, Ti/Al and Ti/Al/Ti/W, are investigated, and it is found that the Ti/W cap layer on Ti/Al leads to low contact resistance with a smooth contact surface morphology. The effect of maintaining unequal mesa and contact pad widths on the extracted values of contact resistance and sheet resistance using the linear transfer length method (LTLM) has been studied. This is important as LTLM structures are used as monitors for process control during various steps of fabrication. It is shown that the extracted contact resistance and sheet resistance values are reliable when the mesa width is equal to the contact pad width. Finally, a possible mechanism for carrier transport in the Ohmic contacts formed using this process has been discussed, based on temperature dependent electrical characterization, and the field emission mechanism is found to be the dominant mechanism of carrier transport. A low Ohmic contact resistance of 0.56 Ω mm, which is one of the lowest reported values for identical metal schemes, and good contact surface morphology has been obtained with moderate post-metal annealing conditions of 600°C.

I. INTRODUCTION

While the technological importance and proliferation of III-nitride high electron mobility transistors (HEMTs) is undisputed, the absence of economically viable and scalable production of bulk GaN wafers led to the development of AlGaN/GaN HEMTs on different substrates such as silicon carbide,[1] sapphire,[2] and silicon (Si). Of these, HEMTs on silicon have been attractive due to economy of scale, better performance at a system level,[3,4] and, very importantly, due to the fact that the existing CMOS foundries can be used for fabricating GaN devices (if the processing technology is also made CMOS compatible), which could significantly bring down the cost of GaN technology.

Ohmic contacts to doped GaN and AlGaN/GaN heterostructures have been studied extensively in the literature.[5] Conventionally, source/drain Ohmic contacts to AlGaN/GaN HEMTs have been fabricated using Au-based metal schemes due to the low values of Ohmic contact resistance obtained.[6–8] A CMOS compatible GaN HEMT process must be Au-free as Au acts as a deep-level trap (recombination center for minority carriers) in silicon and has high diffusion rates in silicon even at moderate temperatures.[9] The other desired features in CMOS compatible GaN process are lower thermal budget, device isolation by ion implantation, and metal deposition by sputtering for good device reliability. Although high temperature post-metal anneal has been shown to produce rough contact surfaces and also lead to long term reliability

issues[10,11] even in Au-based GaN HEMT processes, they are still used due to the low values of contact resistance possible. There are several reports in the literature suggesting various ways of obtaining Au-free Ohmic contact to AlGaN/GaN HEMTs. Some of these reports achieve low contact resistance by using well-engineered metal stacks followed by high temperature post-metal annealing (PMA),[12–14] while others use a pre-Ohmic barrier recess etch, which leads to low contact resistance with even a low temperature PMA step.[3,15–17] Many of the reports on the latter method of forming Au-free contacts explain the effect of annealing temperature and time on the contact resistance, but few reports elaborate on the effect of using different recess etch chemistries, recess etch depths, and metallization on the formation of Au-free, low-temperature sputtered Ohmic contacts to AlGaN/GaN HEMTs.

In this work, we report on the formation of sputtered Au-free Ohmic contacts to AlGaN/GaN heterostructures using different etch chemistries, recess etch depths, and metallization schemes using a moderate annealing temperature of 600 °C. It is found that BCl_3/O_2 etch chemistry leads to more uniformity in electrical characteristics while near-complete recess etching of the barrier in the Ohmic area to the AlGaN/GaN interface and the use of a Ti/Al/Ti/W metal stack lead to optimal contact resistance. The best value of contact resistance and specific contact resistivity obtained in this work is 0.56 Ω mm and 7.26×10^{-6} Ω cm^2, respectively. This is also one of the lowest values of contact resistance reported for similar metal schemes in the literature[17–19] with moderate anneal temperature. In this work, we show that the width of the mesa, formed for achieving electrical isolation between the linear transfer length method (LTLM) structures for recessed Ohmic contacts, should be equal to or less than the contact width for reliable extraction of contact resistance and 2DEG sheet resistance values. This is also supported using Silvaco TCAD simulations. Finally, the carrier transport mechanism responsible for Ohmic behavior of the contacts has been determined using temperature dependent electrical characterization of the contacts, and it is found that the field emission (FE) mechanism is responsible for the Ohmic nature of the recessed gold-free Ohmic contacts discussed in this work.

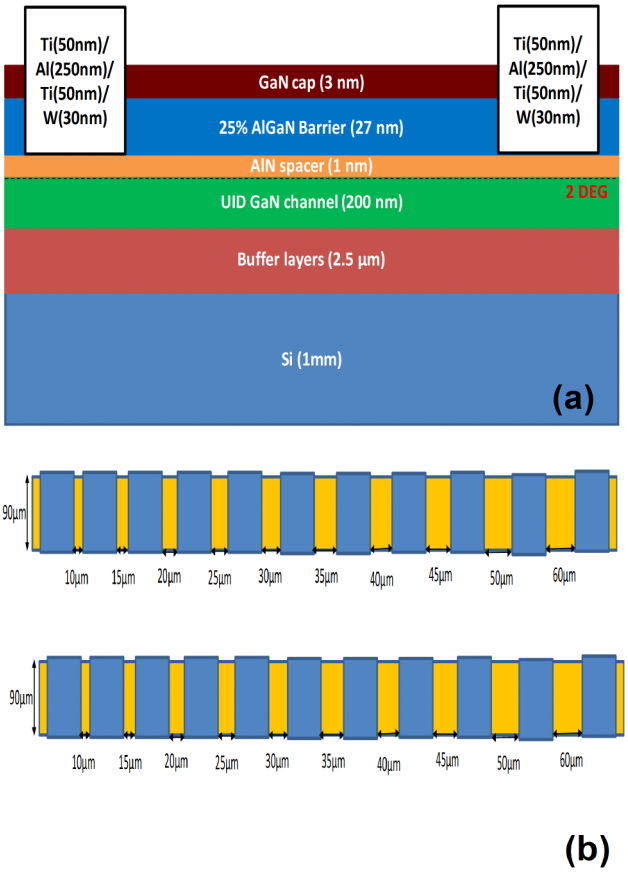

FIG. 1. (a) Schematic cross section of the AlGaN/GaN heterostructure used in this work and (b) schematic cross section of the TLM structures used for extraction of contact resistance.

II. EXPERIMENTAL DETAILS

The AlGaN/GaN wafer used in this work was grown by metal-organic chemical vapor deposition on a 6-in. silicon substrate. The growth details are reported elsewhere.[20] The wafer was diced into several 1×1 cm^2 samples for the purpose of this study. A schematic cross section of the AlGaN/GaN heterostructure samples used in this study and the dimensions of the TLM structures used for extraction of contact resistance are shown in Figs 1(a) and 1(b), respectively.

The samples were degreased in acetone and isopropyl alcohol before fabrication. Contact pads were patterned by optical lithography using AZ4562 photoresist (PR). Using this PR as a soft mask, the AlGaN barrier in the Ohmic contact area was etched down to different depths using different recess etch recipes. Etching was carried out using an OXFORD PlasmaLab 100 ICP/RIE etcher. After a post-recess chemical treatment with dilute HCl, different metal stacks were deposited by sputtering. This was followed by metal lift-off for patterning the contacts. A moderate-temperature post-metal anneal step was carried out on all the samples using rapid thermal annealing with identical conditions of 600 °C for 60 s in N_2 ambient. This was followed by mesa etching for device isolation using AZ5214E as the photoresist soft mask and BCl_3/Cl_2 ICP/RIE dry etch step with an etch rate of 45 nm/min. Standard LTLM structures at different locations across the sample were used to extract the values of sheet resistance and contact resistance. Hall measurements done on van der Pauw structures yielded a sheet resistance of 442 Ω/sq with a 2DEG carrier concentration of $\sim 8 \times 10^{12}$/cm^2. All the electrical measurements reported are done using an Agilent B1500 device analyzer. The AFM scans for etch depth and roughness have been done using a Bruker dimension Icon AFM system or a Park AFM NX 20. The spacing between the contact pads in the TLM structures lies between 10 and 60 μm. The TLM structures used for measurements in all the sections except section D use a TLM pad width of 90 μm, with the mesa width equal to the contact pad width. Since the I–V characteristics increase linearly and saturate beyond a particular applied voltage for smaller TLM spacings, the portion of I–V characteristics between −1 and 1 V is used to determine the resistance values. The

four probe measurement method is used to extract the resistance between the TLM pads accurately.

III. RESULTS AND DISCUSSION

A. Effect of variation in etch chemistry

The most widely used Au-based metal scheme for AlGaN/GaN HEMTs is Ti/Al/Ni/Au.[8,21,22] The formation of Ohmic contact is attributed to the strong reaction at the AlGaN/metal interface leading to the formation of a thin TiN layer, which is thermodynamically favorable. This TiN formation is believed to extract nitrogen from the underlying AlGaN barrier resulting in N vacancies, which leads to heavy n-type doping below the contact area. This fact together with the low work function of interfacial TiN formed is reported as the major reason for Ohmic contact formation.[23] Some of the reports also stress on the importance of formation of Ti-Al alloy phases (predominantly $TiAl_3$) in reducing the contact resistance. There is an additional mechanism suggested in some reports of TiN protrusions spiking into the HEMT stack, which leads to further reduction in the contact resistance when contacts are annealed at higher temperatures (spiking mechanism).[7,21,24] Nickel is used as a diffusion barrier to prevent Al-Au alloy formation, which is known to have high resistivities. All these factors together with the high oxidation resistance and low electrical resistivity of gold lead to optimized Au-based contacts with contact resistances as low as 0.2–0.4 Ω mm.[21–23] With etching of Ohmic area before metal deposition, contact resistances as low as 0.12 and 0.05 Ω mm have been reported.[25,26] In Au-free Ohmic contacts formed at low temperatures without recess etch, composition and thickness of the AlGaN barrier play a crucial role in determining the contact resistance, which generally increases with an increase in the Al composition of AlGaN and an increase in AlGaN barrier thickness. Other complex methods of selective doping below the contact area have also been proposed. A more generalized method to obtain low contact resistance irrespective of the AlGaN barrier used is by pre-Ohmic barrier recess etching.[8,18,23,27–29]

One of the important features of the etch process in this work is the use of a photoresist as a soft mask. The use of soft masks for etching leads to lower process costs and greater flexibility in processing (ease of deposition and removal of the mask). Some of the challenges with using soft masks for low depth recess etch include micromasking, which can lead to higher roughness of etched surface, and sidewall polymer deposition (which is heavily dependent on the etch chemistry and chamber conditions used) impacting the etch profile and depth and the resulting nonuniformity in the electrical characteristics.[30]

Ohmic recess etch reports have mostly used Cl_2,[16] BCl_3/Cl_2,[17–19] or BCl_3 (Ref. 31) chemistries with the addition of Ar or N_2, which may be done to add an additional physical etch component for better etch profile control or for sustaining the plasma as these are low etch rate recipes using low power plasma. Si_3N_4 (Ref. 16) and SiO_2 are the most widely used hard masks.

In this work, we have used BCl_3/O_2 etch chemistry for Ohmic recess etch, which uses separate O_2 and BCl_3 plasma cycles that are repeated alternately for certain number of times to obtain the required etch depth. BCl_3/O_2 chemistry is reported to be a semi-self-limiting etch chemistry for GaN etch, which allows better process control, low roughness, and low etch damage.[32] The O_2 plasma cycle oxidizes a layer of GaN or AlGaN in self-limiting fashion, with the thickness of oxidized GaN layer during a single O_2 plasma cycle increasing linearly with the table RF power. The oxide layer thus formed is etched during the BCl_3 plasma step. BCl_3 is reported to etch oxides better than Cl_2.[33] Moreover, the GaN etch rate using BCl_3 is known to be lesser than Cl_2, which leads to GaN acting as etch stop even if the BCl_3 cycle is prolonged. BCl_3/O_2 chemistry can be especially advantageous when using a soft mask, as an O_2 plasma cycle can effectively reduce the degree of micromasking. Another important advantage of digital etching is the low etch rate/cycle, which makes adaptation of the same recipe for Ohmic recess etching of AlGaN/GaN stacks with different barrier thickness easy (by simply changing the number of etch cycles).

For BCl_3/O_2 digital etch chemistry (recipe 1), O_2 flow rate, RF power, and etch duration of 30 SCCM, 30 W, and 45 s, respectively, were used for the O_2 plasma cycle, while BCl_3 flow rate, RF power, and etch duration of 15 SCCM, 20 W, and 75 s were used for the BCl_3 plasma cycle. Chamber pressure and temperature were maintained at 15 mTorr and 25 °C, respectively.

Another etch recipe with BCl_3/Cl_2 chemistry (recipe 2) was optimized with the same photoresist layer as the soft mask. Initial runs indicated that it is difficult to optimize recess etch with low etch rates of 2–3 nm/min (and acceptable roughness of 1–2 nm) using this chemistry with a soft mask, as the window available for variation of RF power, BCl_3 flow rate, and pressure with sustaining of the plasma is narrow. Achieving a uniform etch with a 2–3 nm/min etch rate using this chemistry might be possible with extensive optimizations, but recipe 2 discussed further has been used for the samples reported in this work.

For recipe 2, the BCl_3 flow rate of 10 SCCM, Cl_2 flow rate of 20 SCCM, and RF power of 5 W was used with the chamber pressure and temperature maintained at 10 mTorr and 25 °C, respectively. The AFM scans for after-etch surface roughness of the Ohmic recess area for recipes 1 and 2 are as shown in Figs. 2(a) and 2(b), respectively. The etch rate and average roughness obtained for the two recipes are tabulated in Table I.

The Ohmic areas on two different samples were etched to a depth of 29–30 nm using the two recipes. Following recess etching, Ohmic contacts were fabricated using sputtered Ti(50 nm)/Al(250 nm)/Ti(50 nm)/W(30 nm) stack and LTLM measurements were done on four sets of structures across the die to check for uniformity in electrical characteristics. The distribution of contact resistance values obtained for four LTLM structures on both the samples is shown in Fig. 3. The obtained contact resistance for recipe 1 was (0.65 ± 0.1) Ω mm while that for recipe 2 was (1.3 ± 0.8) Ω mm. It is clear that when using a soft mask for recess etching, there is wider distribution of extracted contact resistance values across the die when using recipe 2.

To investigate the wider distribution in the values of contact resistance extracted for recipe 2, we carried out AFM scans for quantifying the etch depth uniformity at nine points across the 1×1 cm^2 sample. The etch depth varies approximately from 20 to 30 nm across the nine points. This indicates nonuniformity in the recess etch depth across the die, which may be the reason for variation in the contact resistance values across the sample for recipe 2. This effect is similar to the variation in the threshold voltage of normally off recessed gate HEMTs across the wafer (due to etch

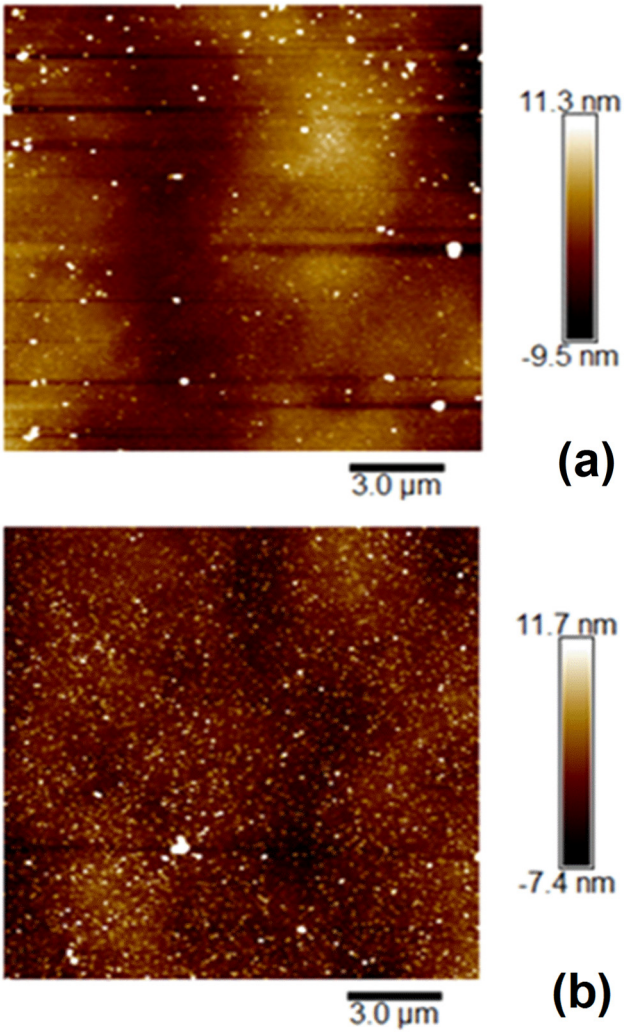

FIG. 2. AFM scans for roughness of (a) BCl_3/O_2 (recipe 1) and (b) BCl_3/Cl_2 (recipe 2) etch chemistries on a scan area of 15 × 15 μm^2.

depth nonuniformity) when BCl_3/Cl_2 recipes are used, in contrast to BCl_3/O_2 recipes.[34] An observation during optimization of the recess etch process was the lower degree of polymerization in BCl_3/O_2 recipes, which can be attributed to factors like the use of an O_2 plasma cycle before each BCl_3 plasma cycle and a wider window for variation of RF power, BCl_3 flow rate, and pressure to arrive at optimum values. Higher degree of uncontrolled polymerization in the BCl_3/Cl_2 chemistry may be one of the reasons for nonuniformity in the etch depth across the sample.

B. Effect of etch depth variation

Various reports have suggested the formation of Ohmic contacts with partial AlGaN barrier recess,[18] complete recess etch of AlGaN barrier,[17,19] and complete recess etch of AlGaN barrier with additional etching of a portion of the unintentionally doped (UID)-GaN channel.[18,35] Due to the wide variety of reports available in the literature, we tried all the three conditions to arrive at the optimum contact resistance. We used BCl_3/O_2 etching with Ti (50 nm)/Al(250 nm)/Ti(50 nm)/W(30 nm) as the Ohmic stack.

We investigated contact resistance corresponding to three recess etch depths using the same metal stack and the same etch chemistry (BCl_3/O_2). In the first case, partial recess etching was done by repeating the digital etch for six cycles to get an etch depth of 18 nm while in the second case, the AlGaN barrier was recess etched completely by using the etching for ten cycles. Both these conditions resulted in Ohmic contacts. The third condition used was a complete recess etch of the AlGaN barrier and a portion of the GaN channel layer, which was implemented by repeating the etching for 15 cycles to get an etch depth of 45 nm. The 15 cycle recess etch resulted in Ohmic contacts too, but the nonuniformity

TABLE I. Etch rate for the two optimized recipes with different chemistries.

Recipe No.	Etch chemistry	Etch rate	Average roughness (nm)	Etch duration
1	BCl_3/O_2	3 nm/cycle	2.2	10 cycles
2	BCl_3/Cl_2	3–4 nm/min (nonuniform across the sample)	1.8	7.5 minutes

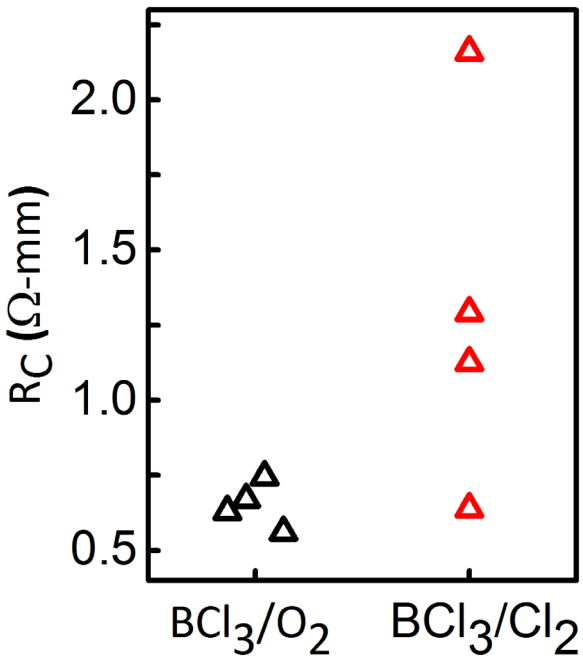

FIG. 3. Distribution of contact resistance obtained for BCl_3/O_2 and BCl_3/Cl_2 etch recipes.

in electrical characteristics was large across the die, with even adjacent sets of contacts showing widely different behaviors. There is one report[16] stating the necessity of an extensively optimized lithography process to get the required sidewall angle profile of the etch with an Si_3N_4 hard mask, so that Ohmic contact can be formed by a direct contact mechanism where the metal contacts the 2DEG directly. This is difficult to achieve using a soft mask. The *I–V* plots and LTLM plots for condition 1 (~18 nm depth) and condition 2 (~30 nm depth) are shown in Figs. 4(a) and 4(b), respectively.

Extracted values of contact resistance, 2DEG sheet resistance, and specific contact resistivities from LTLM structures for conditions 1 and 2 are mentioned in Table II.

The recess etch down to 1–2 nm away from the AlGaN/GaN interface gives a low contact resistance of 0.56 Ω mm compared to a partial recess etch, which gives a higher value of 2.9 Ω mm. This may be due to the additional thickness of the AlGaN barrier layer remaining between the metal contact and the 2DEG in condition 1, which increases the tunneling barrier for electron tunneling, resulting in additional resistance in the current flow path and manifests as an increased value of contact resistance.

The wider distribution in the contact resistance obtained using the BCl_3/Cl_2 etch recipe reported in Sec. III A is further explained by these results. Figure 4(c) shows the possible distribution of contact resistance across the sample based on the etch depths measured across nine locations on the sample and a linear interpolation of the R_C values for etch depth between 18 and 30 nm based on Table II. Although the linear interpolation of the R_C values is not very accurate, it can give a good idea about the possible values of R_C for different etch depths. It can be seen that the distribution of R_C seen in Fig. 3(a) lies within the range of the predicted R_C values by interpolation. This supports the fact that the variation in the R_C for BCl_3/Cl_2 etch chemistry is due to etch depth nonuniformity across the sample.

Since the recess etch of complete AlGaN barrier till the AlN spacer layer gives the optimum contact resistance, BCl_3/O_2 recess etching with an etch depth of 30 nm is used in the processing of the samples, whose results are reported in Secs. III C–III E.

C. Effect of metallization

Electron beam evaporation is widely used for deposition of a contact metal stack on AlGaN/GaN HEMTs for Au-based and Au-free metal schemes;[6,18,24] however, CMOS process lines use sputtering for metal deposition to avoid Si CMOS reliability issues such as increase in oxide charge causing threshold voltage shifts for MOSFETs, increase in leakage through gate oxide and intermetal dielectric, etc. Metal deposition is followed by etching for patterning, rather than lift-off, which is used in III-V industry including standard GaN HEMT processing. In this work, we used sputtering for deposition of the metal stack. We have investigated two metal stacks, Ti/Al and Ti/Al/Ti/W. The metal schemes are examined for two important characteristics; namely, contact resistance and surface morphology. Patterning of the deposited metal is possible either by lift-off or by metal etching. Lift-off is avoided in CMOS processes as it is not a large volume scalable process and also due to low reliability. Metal etching is the preferred method for metal

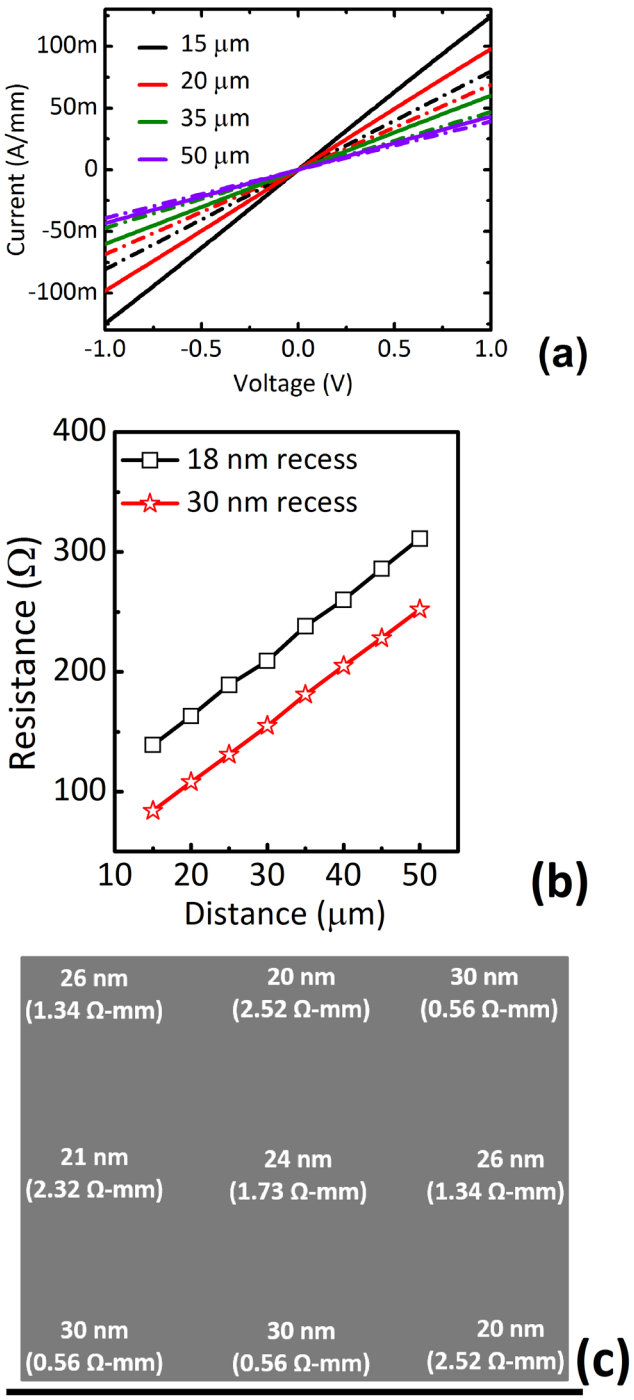

FIG. 4. (a) *I–V* characteristics for contact pad spacing ranging from 15 to 50 μm. The solid lines and dashed lines indicate current levels for 30 and 18 nm recess etched samples. respectively. (b) LTLM plots corresponding to 18 and 30 nm recess etch depths and (c) etch depth and interpolated contact resistance value variation across the 1 × 1 cm^2 sample for the BCl_3/Cl_2 recess etch recipe.

TABLE II. Contact resistance, 2DEG sheet resistance, and specific contact resistivities for the two conditions extracted from LTLM structures.

Condition No.	Etch depth (nm)	Contact resistance (Ω mm)	2DEG sheet resistance (Ω/sq)	Contact resistivity (Ω cm^2)
1	18	2.92	442	1.9×10^{-4}
2	30	0.56	432	7.26×10^{-6}

TABLE III. Contact resistance, 2DEG sheet resistance, and specific contact resistivities corresponding to two different metal stacks.

Stack No.	Metal stack	Contact resistance (Ω mm)	2DEG sheet resistance (Ω/sq)	Contact resistivity (Ω cm^2)
1	Ti/Al/Ti/W	0.56	432	7.26×10^{-6}
2	Ti/Al	1.37	436	4.29×10^{-5}

patterning. Among the metals comprising the metallization stacks investigated in this work, Ti and Al can be etched out by dry etching as they lead to volatile by-products when exposed to chlorine chemistry and the thin layer of W can be etched out by BCl_3 bombardment. Although dry etching of both the metal stacks is possible using BCl_3/Cl_2 chemistry, we have adopted lift-off for our samples reported in this paper. We are in the process of optimizing the etch recipe for the metallization using the BCl_3/Cl_2 chemistry, and the results of the same will be reported in our future works.

The LTLM plots for stack 1 [Ti(50 nm)/Al(250 nm)/Ti(50 nm)/W(30 nm)] and stack 2 [Ti(50 nm)/Al(250 nm] are as shown in Fig. 5.

The extracted values of contact resistance, sheet resistance, and specific contact resistivity for the two stacks are tabulated in Table III.

It is clear from Fig. 5 and Table III that the use of a Ti/W cap layer over the Ti/Al contact layers leads to a reduction in the contact resistance. The reason for this is the reduction in the amount of Al getting oxidized[18] due to the presence of the W cap layer. Another reason may be the reduction in the amount of residual Al (Al left over after Ti-Al alloy formation) due to the presence of a Ti layer on top as well, which can participate in Ti-Al alloy formation. It is well known that the balling up[36] of residual Al when annealed near its melting point leads to degradation in the contact resistance.

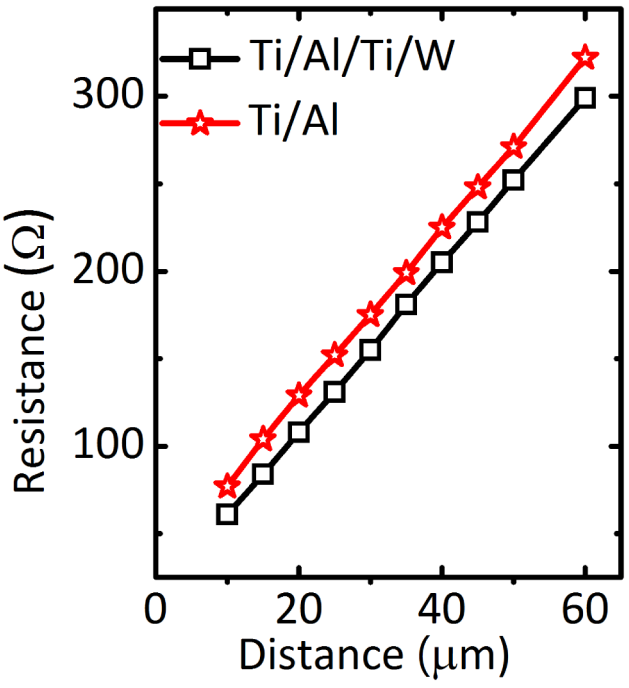

FIG. 5. Comparison between LTLM plots for Ti/Al and Ti/Al/Ti/W metal stacks.

Surface morphology is another important characteristic of a metal contact. In the conventional Ti/Al/Ni/Au process, surface morphology of the contacts is shown to degrade[10,11] due to the high post-metal annealing temperatures used. In this work, a moderate annealing temperature of 600 °C is used. The AFM scans for surface morphology of Ohmic contacts using stacks 1 and 2 post the annealing step are shown in Figs. 6(a) and 6(b), respectively; the average roughness of the metal stacks was found to be 5 and 18 nm, respectively. The contact surface is rougher for stack 2 in comparison to stack 1. Large lumps of metal are observed in the AFM scans for stack 2 (Ti/Al), while such lumps of metal are absent in the scans for stack 1 (Ti/Al/Ti/W). This supports our previous explanation that the top Ti layer participates in alloy formation with the residual Al, thereby reducing the amount of residual Al that can ball up. This indicates another important advantage of using the Ti/W cap layer. Optical images of the Ti/Al/Ti/W and Ti/Al contacts are shown in Figs. 6(c) and 6(d), respectively.

D. Mesa width variation

One of the features of LTLM measurement not often investigated is the effect of mesa width on the extracted value of sheet resistance and contact resistance. To account for lithographic alignment inaccuracies during fabrication, mesa width is usually maintained 5–10 μm greater than the contact width for conventional optical lithography and 3–5 μm greater than the contact width for optical lithography with a stepper. This additional mesa area on either side of the contact pads can affect the extracted values of sheet resistance and contact resistance using the LTLM method.[37] This is because the LTLM method strictly assumes that there is a flow of current only between the contact pads. But, due to recess etching and the proximity of contact metallization to the 2DEG, the electric field due to the voltage applied on the contact pads can spread and control a portion of the 2DEG carriers that are present in the extra mesa region, i.e., voltage on the metal contact can control the 2DEG carriers not only in the area between the contacts but also in the additional mesa area. This can lead to significant

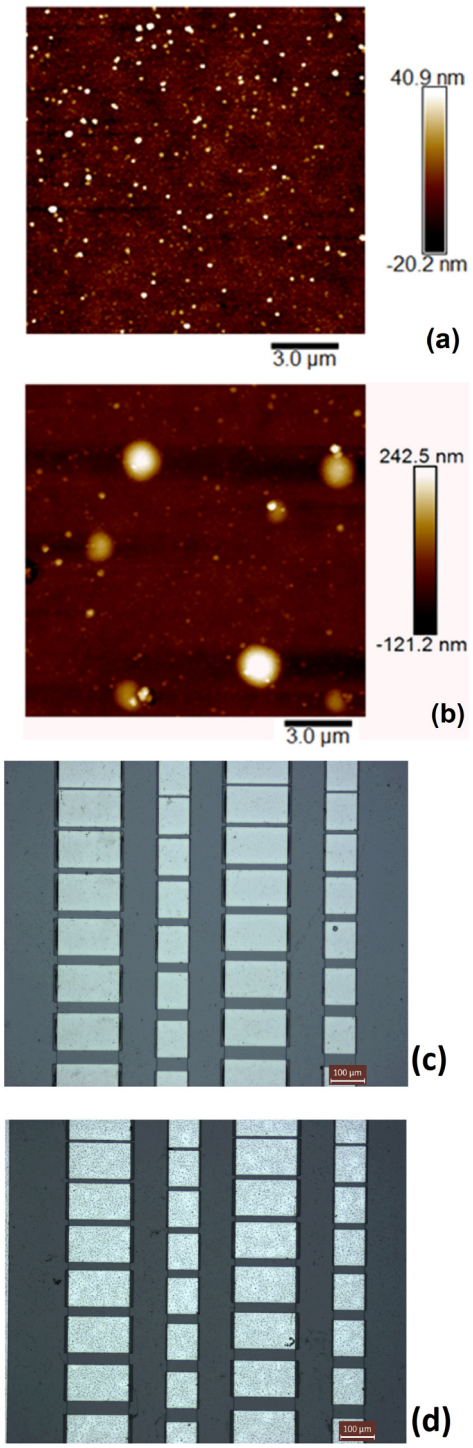

FIG. 6. (a) AFM scans of $15 \times 15\,\mu m^2$ for roughness of Ti/Al/Ti/W (stack 1), (b) AFM scans of $15 \times 15\,\mu m^2$ for roughness of Ti/Al (stack 2) after annealing at 600 °C in N_2 ambient for 60 seconds, (c) optical image of Ti/Al/Ti/W (stack 1), and (d) optical image of Ti/Al (Stack 2).

difference between the values of contact resistance and sheet resistance extracted using LTLM and the actual values.

To ascertain the electric field profile in the LTLM structure and the surrounding mesa region, a portion of the LTLM with a contact area of $100 \times 100\,\mu m^2$, contact spacing of $10\,\mu m$, and mesa width that was $15\,\mu m$ larger than the contact pad width was simulated in Silvaco TCAD. The top view and side view of the 3D device structure as well as electric field distribution along a cut plane across the contact for 10 V of applied voltage is shown in Figs. 7(a)–7(c), respectively. In the simulation, AlGaN thickness is 25 nm everywhere except in the contact area and 1 nm of AlN spacer is placed below the AlGaN and the contact area, followed by the UID GaN layer. AlN below the contact area is n-type doped ($10^{19}\,cm^{-3}$).

It can be seen that the electric field contours/lines are considerably strong and stretch across the 2DEG even beyond the contact area into the portion of the extra mesa width. This indicates an electrostatic control of the contact pad beyond the actual contact area, which can lead to additional current. Hence, the current measured will not only be contributed by the 2DEG sheet charge present between the contact pads but also by the additional 2DEG sheet charge present in the extra mesa area. This is important since LTLM structures are used as process monitors for measurement of contact resistance and sheet resistance during various steps of the device fabrication process. The *I*–*V* simulation of the 3D structure for different mesa widths is shown in Fig. 7(d). It can be seen that as the mesa width is increased (keeping the contact pad width same), the maximum level at which current saturates increases.[38]

To practically study the extent of electrostatic control of the contact over the extra area of the 2DEG and its impact on the extracted contact resistance and sheet resistance, we fabricated LTLM structures using Au-free recessed Ohmic contacts with different mesa widths. We used the BCl_3/O_2 recess etch with Ti/Al/Ti/W stack and post-metal annealing condition of 600 °C for 1 min in N_2 ambient to implement four types of mesa dimensions that are tabulated in Table IV.

The *I*–*V* characteristics measured between pads spaced $15\,\mu m$ apart corresponding to the four different cases of mesa dimension are shown in Fig. 8. It can be seen that there is a significant increase in the current levels when the mesa width is increased. It is noteworthy that the increase in the current levels begins to saturate beyond case 3, which may be due to adequate screening of the applied voltage by the 2DEG electrons within $10\,\mu m$ of the mesa on either side of the contact pad. The exact distance on either side of the contact pads that can be controlled by the applied voltage to the contact may be different for different AlGaN/GaN epi-stacks. This effect is strongly seen in this work since the metallization is close to the AlGaN/GaN interface. The LTLM plots for the four cases are shown in Fig. 9, and the extracted values of sheet resistance and contact resistances have been tabulated in Table V. It can be seen that as the width of the mesa on either side of the contact pads is increased, extracted sheet resistance reduces drastically (which manifests as an increase in the current levels), and the values of extracted contact resistance, contact resistivity, and transfer length increase. If the GaN HEMT process proceeds further and gate metallization is done, this higher level of current may not translate into a higher level of maximum drain current since the gate usually stretches across the entire mesa width.

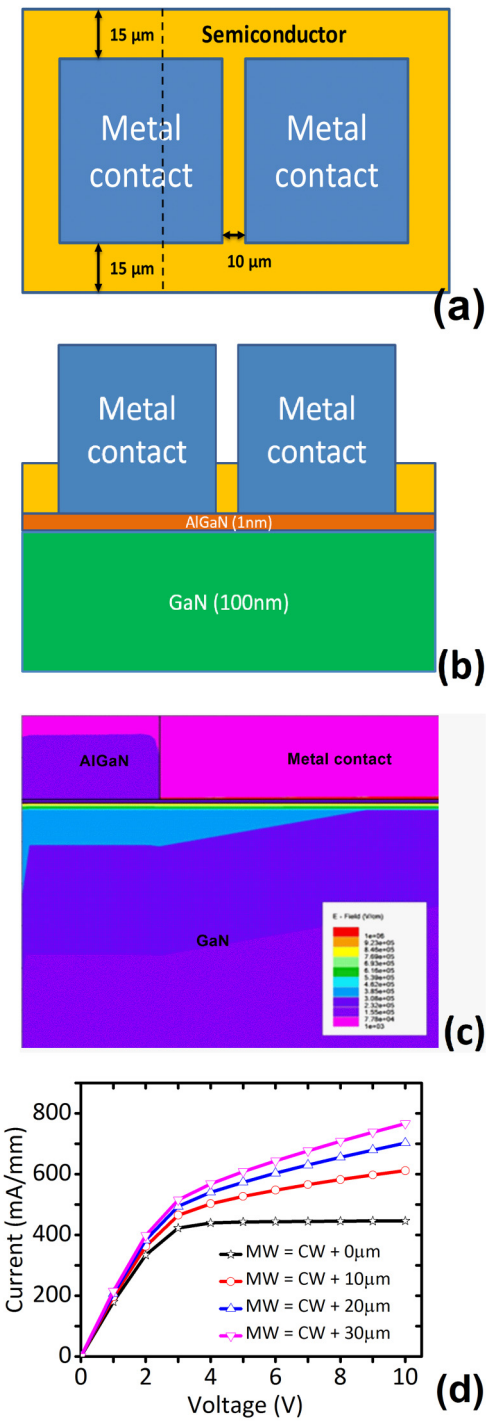

FIG. 7. (a) Top view of the 3D device structure simulated in Silvaco TCAD. (b) Side view of the 3D device structure simulated in Silvaco TCAD. (c) Electric field profile across the cutline shown in (a), and (d) *I–V* characteristics of the 3D-LTLM structure simulated in Silvaco TCAD for contact spacing of 15 μm and contact pad width of 100 μm.

TABLE IV. Conditions of different mesa widths considered in this work.

Case No.	Conditions
1	Mesa width = contact pad width
2	Mesa width = contact pad width + 10 μm
3	Mesa width = contact pad width + 20 μm
4	Mesa width = contact pad width + 30 μm

Nonetheless, LTLM being a prominent method used for monitoring contact resistance and 2DEG sheet resistance during several steps in any fabrication flow, this observation gives an important condition while fabricating these structures in case of recessed Ohmic contacts for extracting the contact resistance and sheet resistance using the LTLM method.

E. Conduction mechanism at metal/semiconductor interface

The conduction mechanism at the metal/semiconductor interface of the Ohmic contact has been explained in the literature by one of the following three mechanisms: thermionic field emission, thermionic emission, and FE.[39] The conduction mechanism for Au-free contacts to AlGaN/GaN HEMTs have been discussed for nonrecessed contact schemes annealed at high temperatures of 850–900 °C (Ref. 40) and for recessed contact schemes annealed at a moderate temperature of 600 °C.[17] In these reports, temperature dependent measurements of the contact characteristics and a plot of specific contact resistivity as a function of temperature have been used to determine this mechanism.

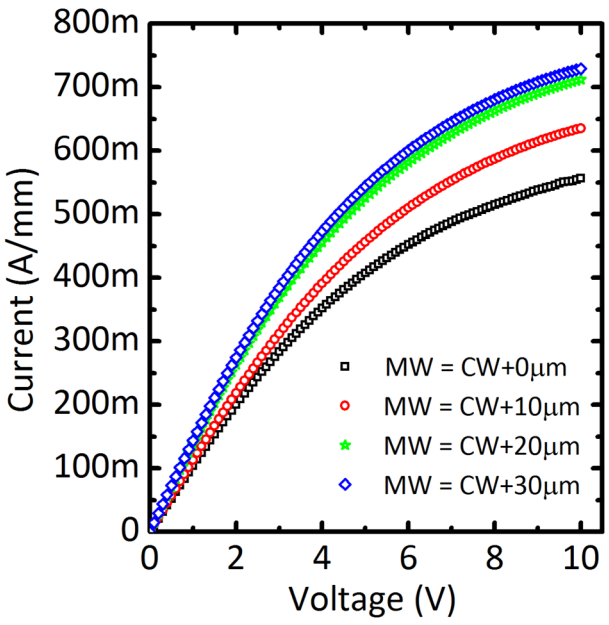

FIG. 8. *I–V* characteristics with 15 μm contact pad spacing for different mesa widths (MW indicates mesa width and CW indicates contact pad width).

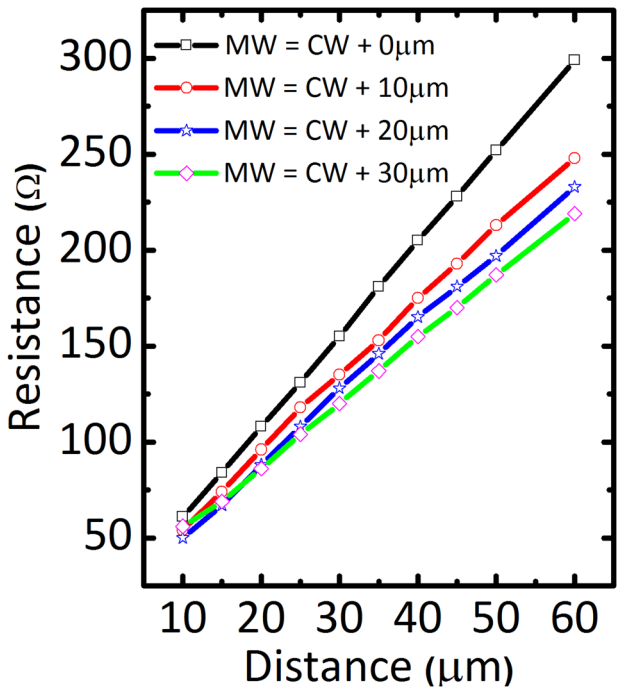

FIG. 9. LTLM plots for different mesa widths (MW indicates mesa width and CW indicates contact pad width).

For the nonrecessed Au-free metallization scheme,[40] thermionic emission is reported as the conduction mechanism at the Ohmic contact. This mechanism is characterized by the strong temperature dependence of specific contact resistivity on temperature. The specific contact resistivity equation for this mechanism is given by Eq. (1),

$$\rho_C = \frac{k_B}{qA^*T}\exp\left(\frac{q\varphi_b}{k_BT}\right), \tag{1}$$

where $k_B$is the Boltzmann constant, A^* is the Richardson constant (26.4 A/cm^2 K^2 for GaN), T is the temperature (in Kelvin), q is the fundamental charge, and φ_b is the barrier height.

TABLE V. Contact resistance, 2DEG sheet resistance, contact transfer length, and specific contact resistivities for different mesa widths.

Case No.	Contact resistance (Ω mm)	2DEG sheet resistance (Ω/sq)	Contact transfer length (μm)	Contact resistivity (Ω cm^2)
1	0.56	432	1.3	7.26×10^{-6}
2	0.87	389	2.23	1.95×10^{-5}
3	0.93	359	2.51	2.34×10^{-5}
4	1.05	332	3.17	3.33×10^{-5}

For the recessed Au-free metallization scheme,[17] field emission has been extracted as the conduction mechanism at the Ohmic contact. The Ohmic contact based on this conduction mechanism is weakly dependent on temperature in comparison to the contacts that operate based on the thermionic emission mechanism. The specific contact resistivity equation for this mechanism is given by Eq. (2),

$$\rho_C = \frac{k_B}{\pi A^*T}\sin(\pi c_1 k_B T)\exp\left(\frac{\varphi_b}{E_{00}}\right), \tag{2}$$

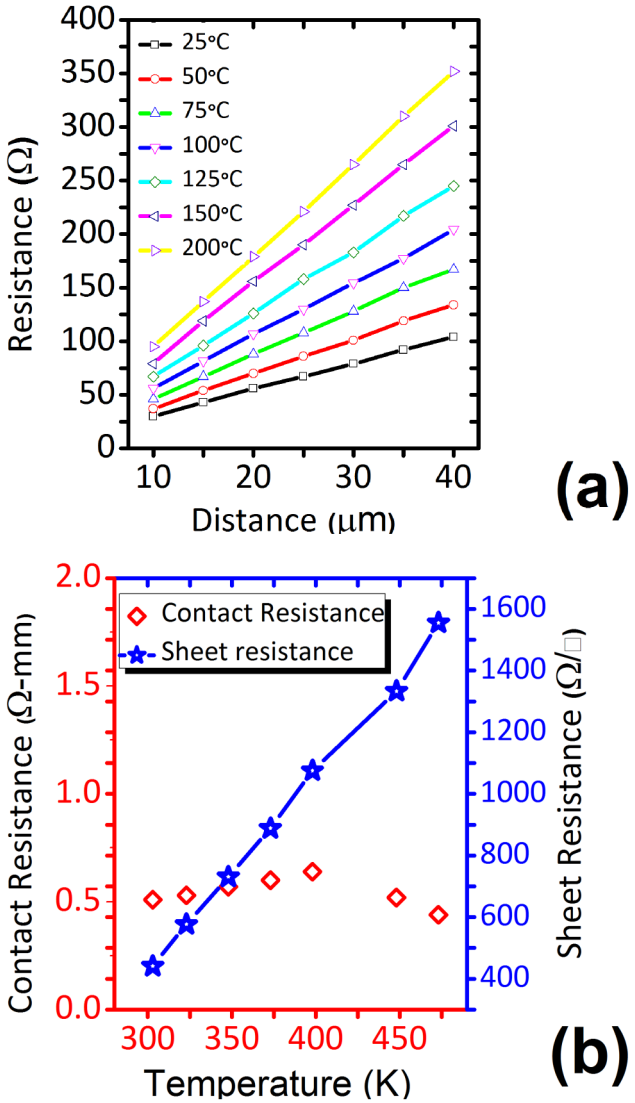

FIG. 10. (a) LTLM plots for different measurement temperatures ranging from 30 to 200 °C and (b) Plot of extracted sheet resistance and contact resistance of TLM structure for different measurement temperatures ranging from 30 to 200 °C.

where

$$c_1 = \frac{\ln\left(\frac{4\varphi_b}{V_n}\right)}{2E_{00}}, \tag{3}$$

$$E_{00} = \frac{hq}{4\pi}\sqrt{\frac{N_D}{m_n^*\varepsilon}}, \text{ and} \tag{4}$$

$$V_n = \frac{k_B T}{q}\ln\left(\frac{N_C}{N_D}\right). \tag{5}$$

N_D is the doping concentration, m_n^* is the effective electron mass ($0.25m_0$ for GaN), ε is the permittivity of GaN ($9\varepsilon_0$), h is Planck's constant, and N_C is the conduction band density of states of GaN.[17]

To investigate the conduction mechanism at the Ohmic contact in this work, temperature dependent measurements of the LTLM structures were carried out with a thermal chuck for measurement at different temperatures. The sample with the Ohmic recess etch using ten cycles of BCl_3/O_2 and the Ti/Al/Ti/W metal scheme was investigated. The temperature dependent LTLM plots are shown in Fig. 10(a). The contact resistance and the sheet resistance as a function of temperature for one of the LTLM structures on the sample are shown in Fig. 10(b).

Specific contact resistivity as a function of temperature has been plotted in Fig. 11, and it is seen that the curve fits well with the field emission model. A barrier height of 0.42 eV and doping concentration of $9.5 \times 10^{18}/cm^3$ are extracted. The fit with the FE model is in good agreement with the data reported by Zhang *et al.*[17] for recessed Ohmic contacts annealed at a moderate temperature. The lower value of barrier height extracted in this work may be the reason for a lower Ohmic contact resistance value obtained in this work.

We explain the formation of an Au-free Ohmic contact to the AlGaN/GaN heterostructure as follows: When titanium comes into contact with the AlN after recess etch, there is nitrogen extraction from underlying GaN during annealing, which leads to nitrogen vacancies in GaN and AlN. Nitrogen vacancy in III-V nitride indicates n-type doping, and it has been stated by many authors that the n-type doping concentration formed during annealing of metallization to AlGaN/GaN heterostructures is high.[41] This leads to the field emission mechanism for carrier transport through the Ohmic contact.

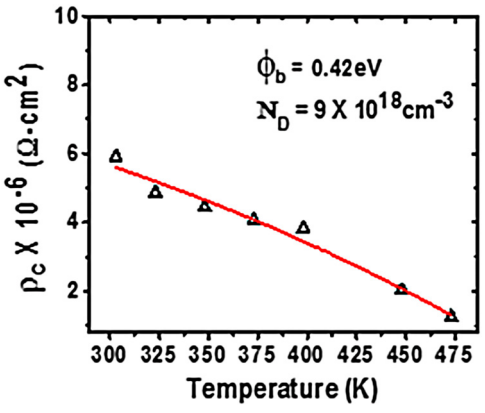

FIG. 11. Specific contact resistivity (ρ_C) vs temperatures ranging from 30 to 200 °C.

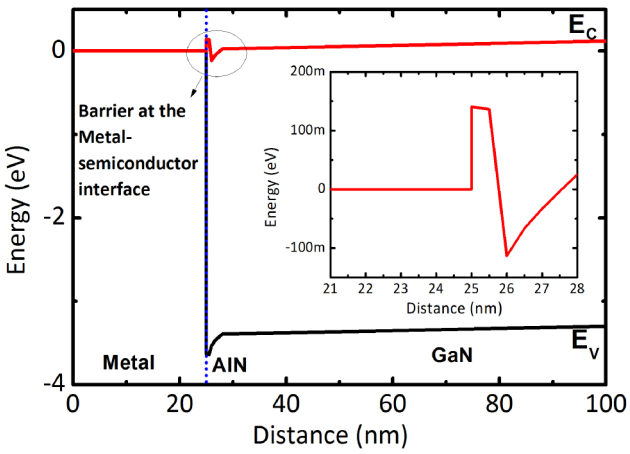

FIG. 12. Possible band diagram at the Ohmic contact-GaN interface simulated in Silvaco (inset shows a magnified version of the conduction band edge). The top line denoted as E_C indicates the conduction band and bottom line denoted as E_V indicates the valence band. The inset shows a zoomed version of the conduction band at the metal-semiconductor interface.

Based on the temperature dependent characterization described above, a representative (not to scale) band diagram at the Ohmic contact interface is shown in Fig. 12. This is the band diagram extracted from the cut-plane used for illustrating the electric field profile in Silvaco TCAD that is described in Sec. III D.

It is also intuitive that due to the barrier height being 0.4 eV and high doping concentration of $10^{19}/cm^3$, field emission should be the only possible conduction mechanism for such type of contacts.

IV. SUMMARY AND CONCLUSIONS

In this work, we have studied recess-etched Au-free Ohmic contacts to AlGaN/GaN HEMTs. It is shown that good uniformity in electrical characteristics across the die is obtained for the BCl_3/O_2 chemistry when using a soft mask. The optimum contact resistance is obtained for a near-complete recess etch of the AlGaN barrier. The use of the Ti/W cap layer on the Ti/Al contact layers is advantageous from the point of view of both lowering the contact resistance and obtaining a low contact surface roughness. We have also shown that the mesa width plays an important role in determining the extracted values of contact resistance and sheet resistance using LTLM structures for recessed Ohmic contacts, with the extracted sheet resistance being significantly affected when the mesa width is larger than the contact width. Finally, we have

TABLE VI. Contact resistance, contact resistivity, and annealing temperature used for similar metal stacks in the literature in comparison to this work.

Reference	Contact resistance (Ω mm)	Contact resistivity (Ω cm^2)	Anneal temperature (°C)
17	1.12	2.77×10^{-5}	600
14	0.358	2.54×10^{-6}	500
19	1.44	5.44×10^{-5}	600
18	0.49	6.5×10^{-6}	870
This work	0.56	7.26×10^{-6}	600

determined the field emission mechanism as the dominant carrier transport mechanism through the metal semiconductor interface, which is responsible for the Ohmic nature of the contacts described in this work. The contact resistance obtained by various authors for a similar metal scheme in the literature has been tabulated in Table VI.

The obtained contact resistance of 0.56 Ω mm is one of the lowest values of contact resistance reported for similar metal stacks in the literature.

ACKNOWLEDGMENTS

The authors acknowledge funding support from MHRD through the NIEIN project and from MeitY and DST through NNetRA. They also acknowledge funding support from ISRO/SCL and IMPRINT-II under SERB. The authors thank the staff and facility technologists at the National Nano Fabrication Facility (NNFC) and the Micro and Nano Characterization Facility (MNCF). The authors acknowledge the help and support of Professor Srinivasan Raghavan and Anirudh Venugopalarao of CeNSE, IISc, Bangalore. The authors also thank Khawaja Nizammuddin Subhani, Facility technologist, NNFC, for his help.

REFERENCES

[1]F. A. Ponce, B. S. Krusor, J. S. Major, W. E. Plano, and D. F. Welch, Appl. Phys. Lett. **67**, 410 (1995).
[2]T. Kozawa, T. Kachi, H. Kano, H. Nagase, N. Koide, and K. Manabe, J. Appl. Phys. **77**, 4389 (1995).
[3]T. E. Kazior, R. Chelakara, W. Hoke, J. Bettencourt, T. Palacios, and H. S. Lee, *Technical Digest—IEEE Compound Semiconductor Integrated Circuit Symposium, CSIC*, Waikoloa, Hawaii, 16–19 October 2011 (IEEE, New York, 2011).
[4]T. E. Kazior, Philos. Trans. R. Soc. A Math. Phys. Eng. Sci. **372**, 20130105 (2014).
[5]G. Greco, F. Iucolano, and F. Roccaforte, Appl. Surf. Sci. **383**, 324 (2016).
[6]F. M. Mohammed, L. Wang, D. Selvanathan, H. Hu, and I. Adesida, J. Vac. Sci. Technol. B **23**, 2330 (2005).
[7]A. Vertiatchikh, E. Kaminsky, J. Teetsov, and K. Robinson, Solid State Electron. **50**, 1425 (2006).
[8]X. Kong, K. Wei, G. Liu, and X. Liu, J. Phys. D. Appl. Phys. **45**, 265101 (2012).
[9]W. M. Bullis, Solid State Electron. **9**, 143 (1966).
[10]D. J. Chen, K. X. Zhang, Y. Q. Tao, X. S. Wu, J. Xu, R. Zhang, Y. D. Zheng, and B. Shen, Appl. Phys. Lett. **88**, 102106 (2006).
[11]M. Piazza, C. Dua, M. Oualli, E. Morvan, D. Carisetti, and F. Wyczisk, Microelectron. Reliab. **49**, 1222 (2009).
[12]Y. Li, G. I. Ng, S. Arulkumaran, C. M. M. Kumar, K. S. Ang, M. J. Anand, H. Wang, R. Hofstetter, and G. Ye, Appl. Phys. Express **6**, 116501 (2013).
[13]A. Constant, J. Baele, P. Coppens, W. Qin, H. Ziad, E. De Backer, P. Moens, and M. Tack, J. Appl. Phys. **120**, 104502 (2016).
[14]T. Yoshida and T. Egawa, Phys. Status Solidi Appl. Mater. Sci. **215**, 1700825 (2018).
[15]J. Zhang *et al.*, IEEE Electron Device Lett. **39**, 847 (2018).
[16]Y. K. Lin *et al.*, Semicond. Sci. Technol. **33**, 095019 (2018).
[17]J. Zhang *et al.*, Appl. Phys. Lett. **107**, 1 (2015).
[18]H. S. Lee, D. S. Lee, and T. Palacios, IEEE Electron Device Lett. **32**, 623 (2011).
[19]Q. Li, Q. Zhou, S. Gao, X. Liu, and H. Wang, Solid State Electron. **147**, 1 (2018).
[20]N. Remesh, N. Mohan, S. Kumar, S. Prabhu, I. Guiney, C. J. Humphreys, S. Raghavan, R. Muralidharan, and D. N. Nath, IEEE Trans. Electron Devices **66**, 613 (2019).
[21]A. Fontserè *et al.*, Appl. Phys. Lett. **99**, 213504 (2011).
[22]K. H. Kim, C. M. Jeon, S. H. Oh, J. L. Lee, C. G. Park, J. H. Lee, K. S. Lee, and Y. M. Koo, J. Vac. Sci. Technol. B **23**, 322 (2005).
[23]G. Greco, F. Giannazzo, F. Iucolano, R. Lo Nigro, and F. Roccaforte, J. Appl. Phys. **114**, 083717 (2013).
[24]L. Wang, F. M. Mohammed, and I. Adesida, J. Appl. Phys. **103**, 093516 (2008).
[25]Y. Lu, X. Ma, L. Yang, B. Hou, M. Mi, M. Zhang, J. Zheng, H. Zhang, and Y. Hao, IEEE Electron Device Lett. **39**, 811 (2018).
[26]M. Meer, A. Rawat, K. Takhar, S. Ganguly, and D. Saha, Microelectron. Eng. **219**, 111144 (2020).
[27]A. Malmros, H. Blanck, and N. Rorsman, Semicond. Sci. Technol. **26**, 075006 (2011).
[28]M. Van Hove, S. Boulay, S. R. Bahl, S. Stoffels, X. Kang, D. Wellekens, K. Geens, A. Delabie, and S. Decoutere, IEEE Electron Device Lett. **33**, 667 (2012).
[29]X. Liu, C. Zhan, K. W. Chan, W. Liu, L. S. Tan, K. J. Chen, and Y. C. Yeo, Appl. Phys. Express **5**, 066501 (2012).
[30]D. S. Rawal, H. K. Malik, V. R. Agarwal, A. K. Kapoor, B. K. Sehgal, and R. Muralidharan, IEEE Trans. Plasma Sci. **40**, 2211 (2012).
[31]A. Constant, J. Baele, P. Coppens, F. De Pestel, P. Moens, and M. Tack, *CS MANTECH 2017—International Conference on Compound Semiconductor Manufacturing Technology*, Indian Wells, CA, 22–25 May 2017 (Indian Wells, CA, 2017), p. 33.
[32]S. D. Burnham, K. Boutros, P. Hashimoto, C. Butler, D. W. S. Wong, M. Hu, and M. Micovic, Phys. Status Solidi Curr. Top. Solid State Phys. **7**, 2010 (2010).
[33]D. Buttari *et al.*, Appl. Phys. Lett. **83**, 4779 (2003).
[34]J. Wu, S. Lei, W.-C. Cheng, R. Sokolovskij, Q. Wang, G. Maggie Xia, and H. Yu, J. Vac. Sci. Technol. A **37**, 060401 (2019).
[35]Z. Liu, M. Heuken, D. Fahle, G. I. Ng, and T. Palacios, *Device Research Conference (DRC) Conference Digest*, June 22–25, 2014 (University of California, Santa Barbara, 2014), p. 75.
[36]A. Motayed, R. Bathe, M. C. Wood, O. S. Diouf, R. D. Vispute, and S. Noor Mohammad, J. Appl. Phys. **93**, 1087 (2003).
[37]H. H. Berger, Solid State Electron. **15**, 145 (1972).
[38]J. Baek, M. S. Shur, K. W. Lee, and T. Vu, IEEE Trans. Electron Devices **32**, 2426 (1985).
[39]S. M. Sze, *Physics of Semiconductor Devices*, 2nd ed. (Wiley, New York, 1982).
[40]Y. Li, G. I. Ng, S. Arulkumaran, G. Ye, C. M. M. Kumar, M. J. Anand, and Z. H. Liu, Appl. Phys. Express **8**, 041001 (2015).
[41]M. Hajłasz, J. J. T. M. Donkers, S. J. Sque, S. B. S. Heil, D. J. Gravesteijn, F. J. R. Rietveld, and J. Schmitz, Appl. Phys. Lett. **104**, 242109 (2014).